Topics in Applied Physics
Volume 112

Topics in Applied Physics

Topics in Applied Physics is a well-established series of review books, each of which presents a comprehensive survey of a selected topic within the broad area of applied physics. Edited and written by leading research scientists in the field concerned, each volume contains review contributions covering the various aspects of the topic. Together these provide an overview of the state of the art in the respective field, extending from an introduction to the subject right up to the frontiers of contemporary research.

Topics in Applied Physics is addressed to all scientists at universities and in industry who wish to obtain an overview and to keep abreast of advances in applied physics. The series also provides easy but comprehensive access to the fields for newcomers starting research.

Contributions are specially commissioned. The Managing Editors are open to any suggestions for topics coming from the community of applied physicists no matter what the field and encourage prospective editors to approach them with ideas.

Managing Editor

Dr. Claus E. Ascheron

Springer-Verlag GmbH
Tiergartenstr. 17
69121 Heidelberg
Germany
Email: claus.ascheron@springer.com

Assistant Editor

Adelheid H. Duhm

Springer-Verlag GmbH
Tiergartenstr. 17
69121 Heidelberg
Germany
Email: adelheid.duhm@springer.com

Andreas Schroeder, Christian E. Willert (Eds.)

Particle Image Velocimetry

New Developments and Recent Applications

With 335 Figures and 24 Tables

Springer

Andreas Schroeder

Deutsches Zentrum
für Luft- und Raumfahrt (DLR)
Institut für Strömungstechnik
und Aerodynamik
Experimentelle Verfahren
Bunsenstrasse 10
37073 Göttingen
Germany
Andreas.Schroeder@dlr.de

Christian E. Willert

Deutsches Zentrum
für Luft- und Raumfahrt (DLR)
Institut für Antriebstechnik
Triebwerksmesstechnik
Linder Höhe
51147 Köln
Germany
chris.willert@dlr.de

Library of Congress Control Number: 2007939493

Physics and Astronomy Classification Scheme (PACS):
42., 47., 51., 83.

ISSN print edition: 0303-4216
ISSN electronic edition: 1437-0859
ISBN 978-3-540-73527-4 Springer Berlin Heidelberg New York
e-ISBN 978-3-540-73528-1 Springer Berlin Heidelberg New York
DOI 10.1071/978-3-540-73528-1

Typesetting: DA-TEX · Gerd Blumenstein · www.da-tex.de
Production: LE-TEX Jelonek, Schmidt & Voeckler GbR, Leipzig
Cover design: eStudio Calamar S. L., F. Steinen-Broo, Girona, Spain

Printed on acid-free paper 57/3180/YL 5 4 3 2 1 0

Preface

The present book provides both a survey of the state-of-the-art of scientific research using particle image velocimetry (PIV) techniques in a wide variety of application fields and also constitutes a synopsis of the main results achieved during the EU funded PIVNET 2 thematic network cooperation. Subtitled with "A European collaboration on development, quality assessment, and standardization of Particle Image Velocimetry for industrial applications" the PIVNET 2 European thematic network has played an important role in the transfer of the PIV technique to industry. Together with PIVNET 1 the network's duration covers a total run time of nearly 10 years during which significant progress on PIV and its applicability was made. The success of this network is due to information exchange, scientific cooperation and synergy effects between the network partners and beyond, stimulated by a multitude of dedicated workshops and actual presentations of PIV in the partner's respective facilities.

The driving force behind these successful networking activities is credited to the initiative and efforts of quite a number of people, who were involved for different periods of time. First of all Michel Stanislas (Laboratoire de Mcanique de Lille) deserves mention as he initiated the cooperation on PIV on the European level by establishing a GARTEUR action group which operated from 1993 to 1995. This activity was later extended to two very successful EC funded research projects: EUROPIV 1 and 2. These projects were devoted to addressing the scientific and technical issues relevant to making the PIV technique operational and feasible in large aeronautical wind tunnels. In the process the need was felt to establish a platform for information exchange on the advantages, prospects and problems of the application of PIV in a much wider range. Thus, the thematic networks PIVNET 1 and later PIVNET 2 were proposed to and subsequently accepted by EC. For more than six years, until the mid-term review of PIVNET 2, both networks were successfully co-oordinated by Jrgen Kompenhans, DLR, before this responsibility was assigned to Andreas Schrder.

The activities of nearly 40 European partners considerably contributed to the fast spreading of the PIV technique in Europe not only to the aeronautical industry including turbomachinery, but also to the car industry, the naval field, the medical and biological fields, as well as household appliances, just to name a few. An important element of conveying the power of the PIV

technique to a broader community have been a variety of demonstrations of its use in industrial facilities, where end users could observe and assess 'real' applications. The idea for such demonstrations was conceived during discussions with Dietrich Knrzer, who supported the network for many years as Scientific Officer. In his succession, Rolando Simonini and Andrzej B. Podsadowski both actively continued with the endorsement of the PIVNET activities.

Two further activities should be mentioned as they were initiated within PIVNET and supported through its funding, and which have grown to a much greater extent than initially anticipated. First, the initiative to bring people performing CFD calculations and experimentalists (here the PIV community) together was motivated to foster the understanding of the problems and possibilities on both sides and to encourage the use of 2D-or 3D velocity data as obtained by PIV for the validation of numerical codes. Lately, precisely this type of close cooperation between numerical and experimental people has gained increasing importance and is becoming a standard procedure.

The second significant initiative started within PIVNET is the establishment of the International PIV Challenge by Michel Stanislas (ERCOFTAC SIG 32) together with the Japanese Flow Visualization Society and colleagues from the United States. Up to now, three different challenges provided a common, standardized platform of comparison and benchmarking for PIV evaluation methods as developed by the leading scientific teams and commercial suppliers. Throughout these activities much knowledge was gained and many ideas for further developments were generated. For prospective end-users of the PIV technique the results of these challenges provide a comprehensive source of information for the assessment of PIV evaluation algorithms.

On the whole the activities associated with the PIVNET 1 and 2 thematic networks, namely the way to promote cooperation, the demonstration of the technique's potential, and the establishment of standards, especially at the evaluation algorithms, may serve as example for other areas where methods developed in the laboratory have the potential to be applied in a wide range of industrial applications.

At this point, the PIV technique is widely spread and differentiated into many distinct applications ranging from micro flows to combustion to supersonic flows, for both industrial needs and research. Based on a relatively simple principle PIV has evolved to a highly versatile flow diagnostics tool and has found realization in many sophisticated technical adaptations. The measurement technique along with the associated hard- and software have improved continuously such that PIV has matured to become a reliable and accurate method for "real life" investigations. The partners of the network have made essential contributions in opening new possibilities for PIV in measurements, scientific research and technology. Nevertheless there is still an ongoing process of improvement and extension of the PIV technique towards time res-

olution, volume-resolved measurements, measurements at micro- and macro-scales, increased accuracy, self-optimizing processing, combinatory measurements with other diagnostics techniques as well as measurements under harsh conditions.

The present book provides a survey of PIV techniques in a variety of application areas corresponding to the workshops organized within PIVNET 2. On this basis outstanding researchers provided a full paper about their specific development, application and/or adaptation of the PIV technique to an experimental investigation within a certain topic of research. In addition, overview articles on the main application topics have been compiled by the workshop organizers or prominent scientists in the respective fields.

Reflecting the network's activities this book is grouped into eleven main topics reviewing the status and potential of the application of PIV to different research fields:

- μPIV and applications to micro systems
- bio-medical flows
- 3D-PIV
- comparison with and validation of CFD
- household appliances
- turbo machinery
- internal combustion
- car industry
- complex aerodynamics
- supersonic flows
- naval applications

The Editors believe that this book serves as a guide through a wide range of research and technology fields in which quantitative flow field data are utilized. It is also an overview of recent improvements and developments in hard- and software and reflects the diversity of applications making use of the powerful PIV technique today. Furthermore this book constitutes the concluding final report of the PIVNET 2 network and shall give valuable information for engineers and physicists facing problems in experimental fluid dynamics using PIV.

The Editors are thankful to all the authors for their efforts in contributing to this book. In the name of the all the involved network partners the Editors acknowledge the financial support of this activity through the European Community. Without doubt this support was a key factor in promoting and disseminating the PIV technique among basic and applied research throughout science and industry.

The compilation and production of this book has been funded by the European Commission within the 5^{th} Framework Programme as part of the PIVNET 2 thematic network (EU GROWTH project G4RT-CT-2002-05081)

Göttingen, Köln *Andreas Schroeder*
December 2007 *Christian E. Willert*

Contents

Measurements and Simulations of the Flow Field in an Electrically Excited Meander Micromixer

Dominik P. J. Barz[1], Hamid Farangis Zadeh[1], and Peter Ehrhard[2]

[1] Research Centre Karlsruhe, Nuclear & Energy Technologies,
P.O. Box 3640, D-76021 Karlsruhe, Germany
dominik.barz@iket.fzk.de
[2] University of Dortmund,
Biochemical & Chemical Engineering, Fluid Mechanics,
Emil-Figge-Str. 68, D-44221 Dortmund, Germany
p.ehrhard@bci.uni-dortmund.de

Abstract. The experimental and numerical verification of the performance of an electrically excited micromixer is the focus of the present work. For the (local) measurement of the flow field within the micromixer we use microparticle image velocimetry (μPIV). Time-dependent and three-dimensional numerical (FEM) simulations, in conjunction with an asymptotic treatment of the electrical double layer, are used as theoretical means. If electroosmotic forces act on the flow, we can, even in straight channel cross sections, resolve complex velocity profiles, which are dominated by electroosmosis close to the walls and by the applied pressure gradient in the channel core. Hence, even flow at walls against the pressure-driven main flow can be observed. Particularly within bends a complex and symmetric flow structure is found, which can be characterized by a number of vortex and saddle points.

1 Introduction

The investigation of mixing and separation processes in microchannels is of great interest with regard to the implementation of such components into lab-on-chip applications. Recent work on mixing, e.g., concentrates on passive mixers, which rely on plane hairpin channels (cf. [1]), on three-dimensional serpentine channels (cf. [2]), or on bas-relief structures on the channel floor (cf. [3]) to achieve centrifugal or chaotic flows, suitable to enhance mixing. Alternatively, active means are employed to induce such secondary flows by, e.g., magnetic forces (cf. [4]) or by electroosmotic forces (cf. [5,6]). Ultimately, all research on efficient mixing or separation in microchannels needs to validate the respective ideas and models. For the experimental validation of such processes, the measurement of velocity and species concentration fields in microchannels appears important.

There are several articles in the literature addressing to some extent the measurement of flow fields in microchannels. The application of laser Doppler anemometry (LDA) in a straight microchannel is discussed, e.g., by [7], featuring a measuring volume of $5\,\mu\text{m} \times 10\,\mu\text{m}$. A LDA profile sensor is outlined

A. Schroeder, C. E. Willert (Eds.): Particle Image Velocimetry,
Topics Appl. Physics **112**, 1–18 (2008)

by [8], reporting a spatial resolution of 1.6 μm. Such a sensor uses two colors to capture both one velocity component and the position of a tracer within a (long) measuring volume and appears promising for microchannels. *Paul* et al. [9] use scalar image velocimetry (SIV) for pressure-driven (and electrokinetic) flows in capillaries and report reliable measurements at a spatial resolution of typically 20 μm. Molecular tagging velocimetry (MTV) is discussed in [10] and applied to the time-dependent interaction of a vortex ring with a wall, whereas the measuring plane has a few centimeters side length. This technique projects an illumination pattern into the liquid and, by a crosscorrelation technique, determines the offset of this (chemically stored) pattern between two moments in time. This technique, likewise, has great potential for application in microchannel flows. The microparticle image velocimetry (μPIV), finally, is the most widely used method to measure velocity fields in microchannels. Introduced in [11] and [12], it employs an epifluorescent microscope to illuminate the complete volume of a microchannel at two given moments in time. The images of the fluorescent particles are then crosscorrelated to obtain offset and velocity fields at a spatial resolution of down to 1 μm in the measuring plane, whereas the "thickness" of the measuring plane can be reduced to 1.5 μm (cf. [11]) or 1.8 μm (cf. [12]). A comprehensive discussion on the spatial resolution of various measuring techniques for the velocity fields in microchannels is conducted in [13]. The μPIV technique has found numerous applications since. Examples are the apparent liquid slip at hydrophobic walls (cf. [14]), the electrokinetic flow excited by dielectric forces (cf. [15]), the mixing of two phases due to hydraulic focusing in microchannels (cf. [16]), and the transition to turbulent flows in straight rectangular (cf. [17, 18]) or straight circular (cf. [19]) microchannels.

We shall concentrate in this chapter on the flow field in an electrically excited micromixer, which has been proposed in [6]. In detail, the authors propose a micromixer comprising a Y-junction and a single meander downstream in the common channel. Mixing is enhanced by applying an alternating electrical field, and hence by superimposing an alternating electroosmotic flow, upon the pressure-driven base flow. The preliminary numerical simulations by [6] demonstrate that, given a reasonable ratio of primary and secondary velocity amplitudes, the time-dependent secondary flow serves to significantly increase mixing quality at the outlet of the device. The present experiments and simulations, therefore, aim to validate the preliminary numerical findings with regard to both velocity and concentration fields. While a concentration-field measuring technique and some concentration measurements are discussed in [20], we shall restrict discussion in this chapter to the velocity field.

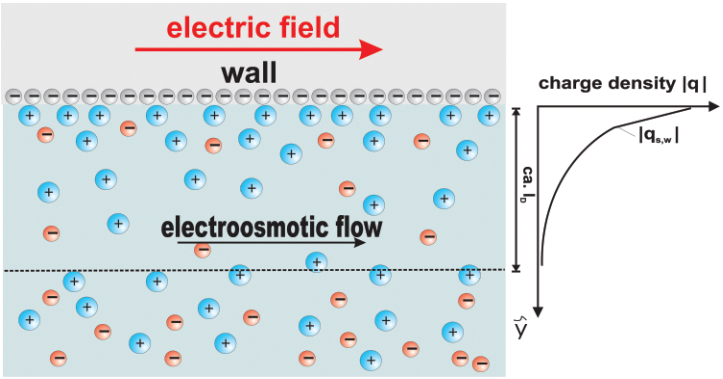

Fig. 1. Physics of electroosmosis

2 Experimental Realization

2.1 Electroosmosis

Before we explain the details of the experimental realization, it appears worthwhile to physically discuss electroosmosis. Given a liquid with mobile charges (e.g., an aqueous solution with ions) adjacent to an electrically insulating solid wall (e.g., glass, plastics), due to chemical/physical interaction we typically find surface charges on the solid. This situation is sketched in Fig. 1. As the surface charges on the solid attract opposite charges out of the liquid, an electrically non-neutral layer of liquid (the so-called electrical double layer, EDL) is the consequence. By applying an electrical field tangentially to the wall, we can introduce electrical forces into this (non-neutral) liquid layer. These forces cause a movement of the liquid – the so-called electroosmotic flow. This effect can be employed in microchannels not only to pump liquids, but likewise to induce secondary flows.

2.2 Experimental Setup

An overview of the experimental setup is presented in Fig. 2. To arrange a flow of liquids through the mixer, we engage a gravity-driven flow with the two inlet reservoirs positioned at a defined height above the outlet reservoir. The liquids are driven through the two inlet channels and leave the micromixer through the common channel. In all cases the flow rates through both inlet channels are identical. As liquid we use deionized water, which has a low electrical conductivity. The low electrical conductivity has two advantages: 1. we minimize electrical currents (due to the applied electrical field) through the liquid, and hence minimize Joule heating, 2. we obtain a thick electrical double layer, and hence pronounced electroosmotic effects. The mass flow rate $\dot{m}$ leaving the common channel is measured by means of a precision balance

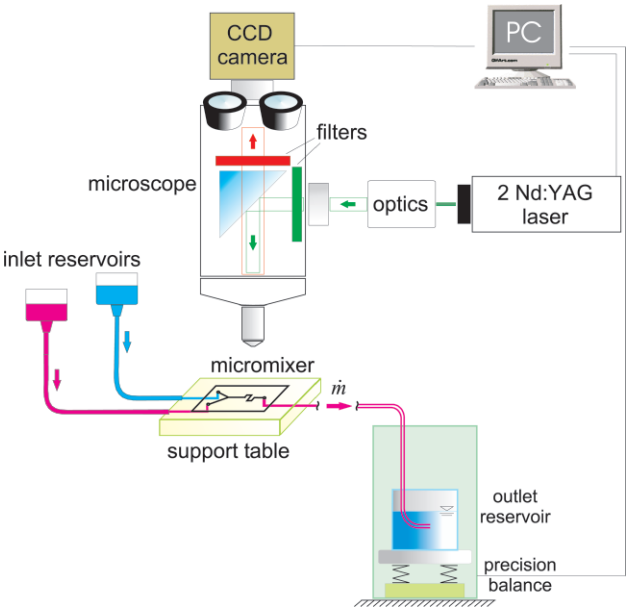

Fig. 2. Sketch of the overall experimental setup

(Sartorius), engaged for time-resolved measurement of the outlet reservoir mass. This balance has an accuracy of $\pm 0.01\,\mathrm{mg}$ and submits the data via a RS232 serial interface to a PC, where LabVIEW (National Instruments) handles the processing of the data. The gravity-driven delivery system is calibrated by mass-flow measurements at several flow rates. First, in the outlet reservoir the evaporation rate of the water is measured. Secondly, after connecting all reservoirs, the levels of the inlet reservoirs are adjusted at different heights above the outlet reservoir, namely in the range $0 \leq \Delta h \leq 100\,\mathrm{mm}$. The measured mass flow rates $\dot{m}$ are measured and corrected by the evaporation rate (typically $\dot{m}_{\mathrm{ev}} \simeq 20\,\mu\mathrm{g/s}$). This method ensures an accuracy for the mass flow rate of better than $\pm 3\,\mu\mathrm{g/s}$. From the mass flow rates, the volumetric flow rates $\dot{V} = \dot{m}/\rho$ are obtained at known density ρ. This defines the Reynolds number for the rectangular (square) common channel

$$\mathrm{Re} = \frac{\bar{u}d}{\nu}\,, \tag{1}$$

with the mean velocity $\bar{u} = \dot{V}/d^2$ and the kinematic viscosity of the liquid ν. We use temperature-dependent data for density and viscosity. In summary, the (steady) forced flow through the micromixer will be characterized by the Reynolds number. The Reynolds numbers in (1) is valid for the common channel, whereas both inlet channels are characterized by half the Reynolds number.

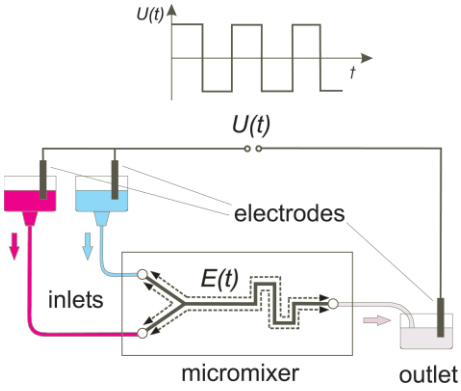

Fig. 3. Arrangement of electrodes for the buildup of the electrical field

2.3 Electrical Excitation

In parallel with the (steady) forced flow, we apply a time-dependent electrical field to set up an electroosmotic flow. The arrangement for the electrical field buildup is sketched in Fig. 3. A DC power supply and an amplifier allow to us apply potential differences of up to 5 kV. Gold electrodes are placed in the inlet and outlet reservoirs. One potential is connected to both inlet reservoirs, the second potential is connected to the outlet reservoir. This arrangement sets up an electrical field, which is roughly directed tangentially to the channel axis. A function generator in conjunction with a relay exchanges the polarity of all electrodes periodically in time at a defined frequency (typically 0.1 Hz). This provides a local electrical field in the channel, alternating in a square-signal fashion. The electrical signal from the function generator is, moreover, used for triggering purposes. In detail, the triggering is necessary to record phase-correctly multiple velocity fields for averaging.

2.4 Micromixer

The micromixer under investigation (cf. Fig. 3) features a Y-form joining of two inlet channels, followed by a straight common channel with a single meander downstream, all realized in FOTURAN glass (cf. [21]). The channels of the Y-mixer and the meander channel, all have square cross sections of 110 µm × 110 µm. At the Y-mixer, the merging channels comprise an angle of 40°, while the meander is located 17 mm downstream of this point. A closeup sketch of the meander is given in Fig. 4.

2.5 Optical Measurement Technique

The micromixer, mounted on the support table, allows for optical access via an inverted microscope (Leica, DMIRM). A number of microscope objectives (Leica, NPLANL, HCPLFL) with different magnification M and numerical

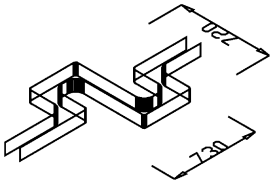

Fig. 4. Closeup sketch of the meander part; measures are given in μm

aperture NA, all accommodated for air, is mounted onto the microscope, depending on the actual field of interest.

We aim to perform flow-field measurements through this microscope by means of the so-called microparticle image velocimetry (μPIV), which is described in detail, e.g., in [11] or [12]. For that reason we engage a fluorescence technique as sketched in Fig. 5. Two Nd:YAG lasers (New Wave, Solo-PIV) provide two pulses of green light ($\lambda_\mathrm{i} = 532\,\mathrm{nm}$), which are expanded and coupled into the coaxial illumination path of the microscope. Hence, we obtain green volume illumination of the microchannel. Within the flow a mixture of fluorescent microspheres of diameter 200 nm and 500 nm (Duke Scientific) is suspended. The density of the microspheres ($\rho = 1.05\,\mathrm{g/cm^3}$) is well adjusted to the water density. The microspheres are customized for emission in the red regime, i.e., at a wavelength around $\lambda_\mathrm{e} \simeq 612\,\mathrm{nm}$. The red light from the microspheres passes the epifluorescent cube within the microscope and is imaged onto the CCD camera. In contrast, green reflected light is blocked by the epifluorescent cube from reaching the CCD camera. We use a high-performance cooled interline CCD camera (PCO, Image Intense) with 1376×1040 pixels and 12-bit readout resolution to record the double frames. The acquired double frames from the camera are transferred to a PC, the software DaVis6.2 (LaVision) is applied for further processing. All timing, synchronization, and control of the camera and the lasers is achieved by a programmable timing unit (PTU) card, installed in the PC, in conjunction with the DaVis software.

We typically subdivide the total area occupied by the fluid into interrogation areas of 16×16 pixels ($4.8\,\mu\mathrm{m} \times 4.8\,\mu\mathrm{m}$), whereas the computation of the displacement vector within each interrogation area of the double frames is based on a crosscorrelation method within the DaVis software. We keep the ratio of microsphere volume and fluid volume in the range 0.05–0.07 % to ensure by this moderate concentration of microspheres a high signal-to-noise ratio. This gives typically around 5 microspheres per interrogation area. We use in all cases ensemble averaging of typically 20–40 single crosscorrelation functions, to improve the accuracy of the measured flow fields (cf. [22]). As we have a periodically alternating electrical field, we can expect likewise a periodically oscillating flow field. Hence, a phase-correct sampling of the flow field during a large number of alternation periods (20–40) is established, which uses the electrical signal from the electrodes for triggering. The fre-

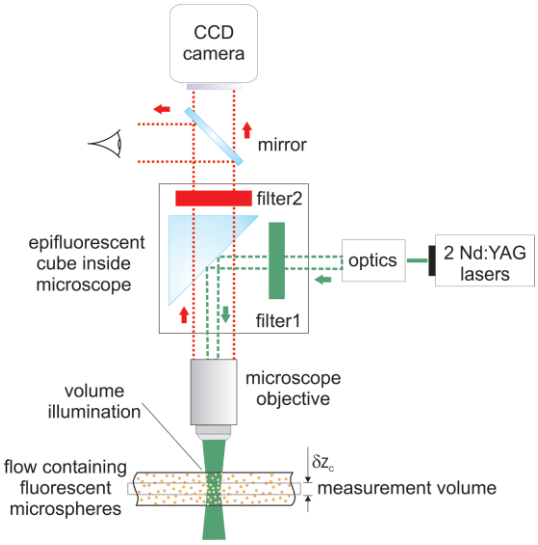

Fig. 5. μPIV setup for microflow investigations

quency of alternation in all cases is 0.1 Hz, i.e., each 5 s the direction of the electrical field is inverted. Accordingly, the double frames are recorded with a small time offset in the range $\Delta t \leq 10$ ms in all cases.

In contrast to conventional PIV, with the thickness of the lightsheet defining the measuring volume, the illumination within the μPIV setup is responsible for an unsharp measuring volume, resulting from the focal plane and the depth of field. Following [22], the thickness of the measuring volume should rather be defined from the so-called depth of correlation than from the pure depth of field. *Meinhart* et al. [22] estimate the depth of correlation by

$$\delta z_{\mathrm{c}} = \frac{3n\lambda_{\mathrm{e}}}{\mathrm{NA}^2} + \frac{2.16 d_{\mathrm{p}}}{\tan\theta} + d_{\mathrm{p}}\,. \tag{2}$$

In (2) n is the refractive index of the medium between the microchannel and the objective, λ_{e} is the emitted light wavelength, NA is the numerical aperture of the objective, d_{p} the particle diameter, and θ is the collection angle of the optical system. For the present measurements the depth of correlation is $\delta z_{\mathrm{c}} \simeq 16\,\mu$m.

Particles, as used for the μPIV technique, in principle experience electrophoretic forces if subjected to an electrical field. The electrophoretic velocity is checked in a (separate) sealed microchannel of identical cross section and subjected to identical electrical field conditions. For these experiments, particles of diameter $d_{\mathrm{p}} = 0.2\,\mu$m and $1.0\,\mu$m are used, giving velocity amplitudes of up to $7.7\,\mu$m/s and $5.8\,\mu$m/s, respectively. This choice of particles is made to cover a, preferably wide, range of sizes. In both cases this is smaller

than 0.7 % of the electroosmotic velocity amplitude and therefore the electrophoretic contribution can be neglected in the remainder of the chapter.

3 Theoretical Model

The numerical simulations of flow and transport within the micromixer rely on the time-dependent and three-dimensional Navier–Stokes equations and the continuity equation. Hence, for an incompressible Newtonian liquid we have

$$\nabla \cdot \boldsymbol{v} = 0\,, \tag{3}$$

$$\rho\left[\frac{\partial \boldsymbol{v}}{\partial t} + (\boldsymbol{v}\cdot\nabla)\boldsymbol{v}\right] = -\nabla p + \mu\Delta\boldsymbol{v} - q\nabla\varphi\,. \tag{4}$$

For a poorly conducting liquid, further, the Gaussian law

$$\nabla\cdot(\epsilon_r\nabla\varphi) = -\frac{q}{\epsilon_0} \tag{5}$$

holds. For the electrical charge distribution q within the (thin) electrical double layer (EDL) we can, moreover, invoke the Debye–Hückel approximation

$$q \simeq \frac{q_\zeta}{l_\mathrm{D}}\exp\left(-\frac{z}{l_\mathrm{D}}\right). \tag{6}$$

Within the above equations we engage a local coordinate system, with the origin on the wall. Hence, x and y are the wall-tangential coordinates and z is the wall-normal coordinate. Further, $\boldsymbol{v}$ is the fluid velocity vector, ρ denotes density, p pressure, μ dynamic viscosity, φ the electrical potential, $\epsilon_0\epsilon_r$ the respective dielectric properties, q_ζ the charge density at the boundary between shear layer and Gouy–Chapman layer (within the EDL), and l_D the Debye length.

The boundary conditions require no slip and a prescribed electrical potential, according to the Debye–Hückel approximation, at all channel walls. Hence, we have

$$\boldsymbol{v}(x,y,0) = 0\,, \tag{7}$$

$$\varphi(x,y,0) = -\frac{q_\zeta l_\mathrm{D}}{\epsilon_0\epsilon_r}. \tag{8}$$

We restrict our simulations to the meander segment of the micromixer and exclude the Y-mixer segment. Hence, we need to formulate boundary conditions within the inlet and outlet cross sections. We assume in both cross sections a pressure-driven fully developed and unidirectional flow; for a rectangular channel the developed-flow profile follows a series solution (cf. [23]). Further, the electrical potential at the inlet and outlet cross section is inferred

from the time-dependent electrical potential at both electrodes. Hence, we have

$$u_{\text{in}}(y,z) = -\frac{1}{2\mu}\frac{\mathrm{d}p}{\mathrm{d}x}\left[\left(\frac{d^2}{4}-y^2\right) - \frac{8}{d}\sum_{n=0}^{\infty}\frac{(-1)^n}{N_n^3}\frac{\cosh(N_n z)}{\cosh(N_n d/2)}\cos(N_n y)\right], \quad (9)$$

$$v_{in} = 0\,, \qquad w_{in} = 0\,, \quad (10)$$

$$\frac{\partial u_{\text{out}}}{\partial x} = 0\,, \qquad v_{\text{out}} = 0\,, \qquad w_{out} = 0\,, \quad (11)$$

$$\varphi_{\text{in}} = f_1(t)\,, \qquad \varphi_{\text{out}} = f_2(t)\,, \quad (12)$$

whereas $N_n = (2n+1)\pi/d$ and $f_1(t)$, $f_2(t)$ are of square-signal type and phase shifted by π.

We treat the above system (3)–(12) in nondimensional form by introducing the (channel) scales

$$(X,Y,Z) = \frac{(x,y,z)}{d}\,, \quad (U,V,W) = \frac{(u,v,w)}{\bar{u}}\,, \quad (13)$$

$$\tau = \frac{t}{(d/\bar{u})}\,, \quad P = \frac{p}{(\mu\bar{u}/d)}\,, \quad \Phi = \frac{\varphi}{\varphi_0}\,. \quad (14)$$

Thus, lengths are scaled by the width d and velocities by the average (pressure-driven) velocity $\bar{u}$ of the microchannel. Further, a transport time-scale and a viscous pressure scale is used; the electrical potential is scaled by the applied potential difference φ_0. Due to the nondimensionalization, beyond the Reynolds number (cf. (1)), a number of dimensionless groups arise, namely

$$\delta = \frac{l_d}{d} \ll 1\,, \quad \Pi = \frac{q_\zeta \varphi_0}{\mu\bar{u}}\,. \quad (15)$$

The Reynolds number Re characterizes the pressure-driven flow through the micromixer, δ is a ratio of length scales, and Π is the ratio of electrical and viscous forces, characterizing the strength of the electroosmotic flow.

Due to largely different length scales ($\delta \ll 1$), it appears reasonable to seek, by asymptotic means, an inner solution, valid within the EDL, and an outer solution, valid within the channel core; the details of this procedure are given by [6]. The inner solution can be given analytically, the outer solution is obtained by the standard finite-element code FIDAP. It is important to note that, for the outer solution, there remains no need to resolve the EDL numerically. The matching and superposition of both solutions provides an approximation for the solution in the entire domain. The finite-element simulations for the channel core are time dependent and three-dimensional in nature.

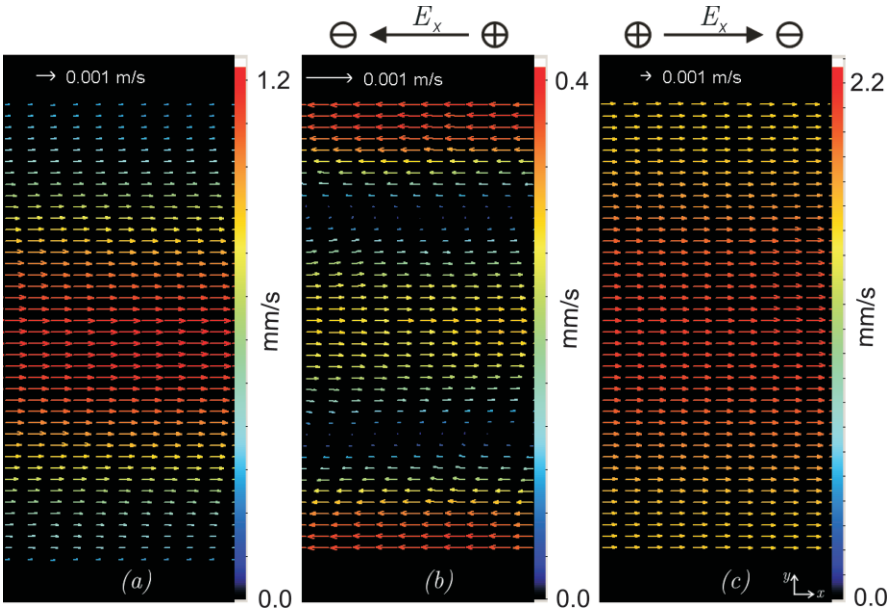

Fig. 6. Velocity fields of the flow at Re $\simeq 0.1$ at the level $z/d = 0.25$ in the straight channel of the micromixer: (**a**) without electrical field, (**b**) subject to an electrical field $E_x \simeq -14.5\,\mathrm{V/mm}$, and (**c**) $E_x \simeq +14.5\,\mathrm{V/mm}$. The velocity amplitudes are color coded, according to the given color tables at each part of the figure

4 Results

The setup, the μPIV measurements, and the numerical simulations are engaged to study the flow in various parts of the micromixer, with and without electrical excitation. The results in this section cover the electroosmotic flow 1. in the straight channel and 2. within the meander bends of the micromixer.

4.1 Electroosmotic Flow in the Straight Channel of the Micromixer

All measurements in this section are taken in the straight channel of the glass micromixer, which is located between the Y-junction and the meander. The precise position is 15 mm downstream of the Y-junction, all cross sections are $110\,\mu\mathrm{m} \times 110\,\mu\mathrm{m}$. We establish a pressure-driven flow by applying a pressure difference of $\Delta p \simeq 157\,\mathrm{Pa}$ between both inlet reservoirs and the outlet reservoir. This results in a Reynolds number of Re $\simeq 0.1$ in the common channel. This weak pressure-driven flow is chosen to have both the pressure-driven flow and the contingent electroosmotic flow at similar velocity amplitudes. Hence, the superposition of both flows makes a real (measurable) difference.

The result for the pure pressure-driven flow at the level $z/d = 0.25$ is given in Fig. 6a. The origin of the coordinate system is on the channel axis, with x pointing downstream along the channel axis and y and z orthogonal to the channel axis, pointing in horizontal and vertical directions. Hence, $z/d = 0.25$ is exactly between the midheight level and the top wall. The velocity vectors in Fig. 6a are based on an ensemble average of the crosscorrelation functions of 40 double frames, with a time interval of $\Delta t = 2\,\mathrm{ms}$ between the two images of each double frame. The microscope objective has a magnification of 20×, featuring a depth of correlation (cf. (2)) of $\delta z_\mathrm{c} \simeq 16\,\mu\mathrm{m}$ for the given particle size. Interrogation areas of 16×16 pixels ($4.8\,\mu\mathrm{m} \times 4.8\,\mu\mathrm{m}$) are engaged with an overlap of 50 %. We recognize a steady flow profile, parallel to the walls, with a maximum velocity of about 1.2 mm/s in the middle of the channel ($y = 0$), and vanishing velocities at the walls. This profile appears roughly parabolic.

To excite an electroosmotic flow, we apply a potential difference of 1.0 kV between the inlet reservoirs and the outlet reservoir (cf. Sect. 2.3), alternating at a frequency of 0.1 Hz. This causes an electrical field of strength $|E_x| \simeq 14.5\,\mathrm{V/mm}$, directed tangentially to the channel axis and inverting its direction every five seconds. For all measurements we trigger the first image of the double frame at 4.5 s after the switch of polarity, while the time interval between two images of a double frame remains $\Delta t = 2\,\mathrm{ms}$. After each switch of polarity the flow needs less than two seconds to adjust to the new electrical field direction. Hence, between two and five seconds after the switch of polarity a quasisteady flow persist. In summary, we sample phase-correctly multiple measurements of the flow field at the end of the quasisteady period and ensemble average the crosscorrelation functions of 40 double frames. The results are given in Figs. 6b,c.

During the period of a negatively directed electrical field with $E_x \simeq -14.5\,\mathrm{V/mm}$ (cf. Fig. 6b) we find close to both walls of the microchannel electroosmotic flow into the negative x-direction, i.e., against the pressure-driven flow. In the middle of the channel ($y = 0$), due to the pressure field, the flow is in the positive x-direction, again featuring a roughly parabolic profile around the middle region. Hence, negative velocities of up to $u \simeq -0.6\,\mathrm{mm/s}$ are found near the walls, while positive velocities of up to $u \simeq +0.4\,\mathrm{mm/s}$ are found in the middle of the channel. During the period of a positively directed electrical field with $E_x \simeq +14.5\,\mathrm{V/mm}$ we find the flow field given in Fig. 6c. Here, near both walls an electroosmotic movement of the liquid into the positive x-direction is obvious, rapidly rising to velocities of $u \simeq 1.4\,\mathrm{mm/s}$ across a thin wall layer. This leads to larger velocities of up to $u \simeq 2.0\,\mathrm{mm/s}$ in the middle of the channel. The roughly parabolic form of the velocity profile in the channel core appears to be preserved.

It is obvious from Figs. 6b,c that the electrical field causes movement of the liquid near the walls in either direction, depending on the direction of the electrical field. The combination of glass and water is characterized by negative electrical charges at the glass surface (wall). The negatively charged

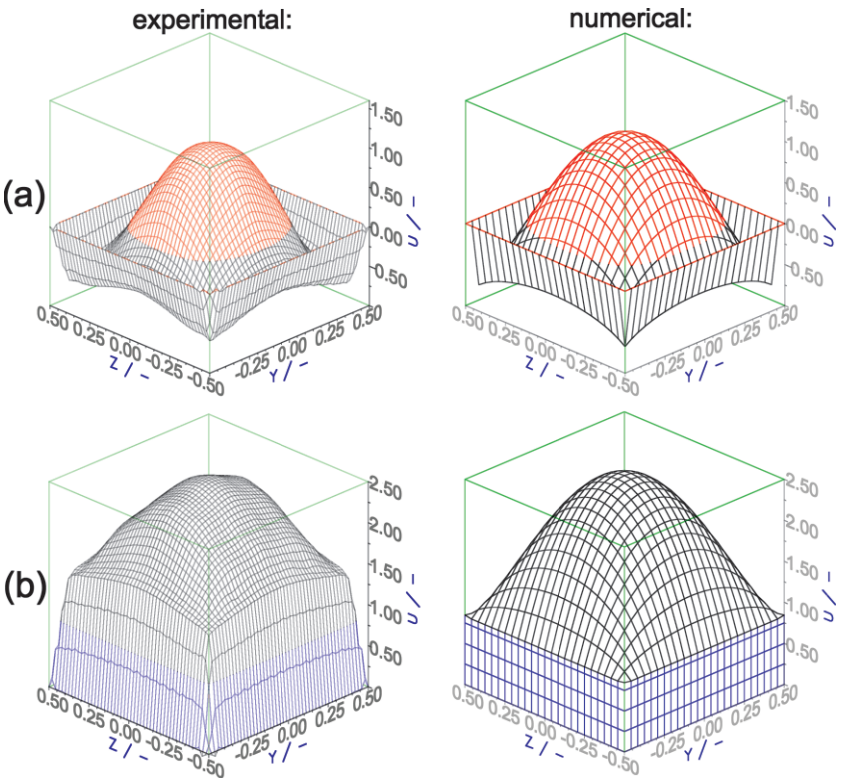

Fig. 7. Axial velocity profiles of the flow at Re $\simeq 0.1$ for the straight channel of the micromixer: (**a**) subject to an electrical field of $E_x \simeq -14.5\,\mathrm{V/mm}$ and (**b**) subject to an electrical field of $E_x \simeq +14.5\,\mathrm{V/mm}$

wall accumulates positive charges (e.g., H_3O^+ ions) next to the wall, leading to a positively charged layer in the liquid – the electrical double layer (EDL). The application of a positively directed electrical field causes forces on the ions in the EDL, which tend to move these ions (and the layers) towards the electrode at the outlet, i.e., in the positive x-direction. The opposite direction of the electrical field inverts the forces onto the wall layer and a complex velocity field, directed at the walls in the negative x-direction and in the middle of the channel in the positive x-direction, is the consequence.

In addition to the measurements in a specific level, we have performed velocity measurements in 15 levels of the microchannel in the range $-0.5 \leq z/d \leq 0.5$. This allows us to infer, e.g., the axial velocity field within the complete cross section of the microchannel. For these measurements all optical and evaluation parameters and procedures remain unchanged, an overlap of the interrogation areas, however, is avoided. In order to verify the measuring technique, the measured flow field of the pure pressure-driven flow has been compared with the analytical series solution for the laminar flow in